Human Molecular Genetics, 2021, Vol. 30, No. 23 2300–2314

https://doi.org/10.1093/hmg/ddab192
Advance Access Publication Date: 10 July 2021
General Article

GENERAL ARTICLE

KCND2 variants associated with global developmental delay differentially impair Kv4.2 channel gating

Yongqiang Zhang[1,2], Georgios Tachtsidis[1], Claudia Schob[3], Mahmoud Koko[4], Ulrike B.S. Hedrich[4], Holger Lerche[4], Johannes R. Lemke[5,6], Arie van Haeringen[7], Claudia Ruivenkamp[7], Trine Prescott[8], Kristian Tveten[8], Thorsten Gerstner[9,10], Brianna Pruniski[11], Stephanie DiTroia[12], Grace E. VanNoy[12], Heidi L. Rehm[12], Heather McLaughlin[13], Hanno J. Bolz[14,15], Ulrich Zechner[14,16], Emily Bryant[17], Tiffani McDonough[17], Stefan Kindler[3] and Robert Bähring[1,*]

[1]Center for Experimental Medicine, Institute for Cellular and Integrative Physiology, University Hospital Hamburg-Eppendorf, 20246 Hamburg, Germany, [2]Southeast University, Nanjing 210009, China, [3]Institute for Human Genetics, University Hospital Hamburg-Eppendorf, 20246 Hamburg, Germany, [4]Department of Neurology and Epileptology, Hertie-Institute for Clinical Brain Research, University of Tübingen, 72076 Tübingen, Germany, [5]Institute of Human Genetics, University of Leipzig Medical Center, 04103 Leipzig, Germany, [6]Center for Rare Diseases, University of Leipzig Medical Center, 04103 Leipzig, Germany, [7]Department of Clinical Genetics, Leiden University Medical Center, 2333 Leiden, The Netherlands, [8]Department of Medical Genetics, Telemark Hospital Trust, 3710 Skien, Norway, [9]Department of Child Neurology and Rehabilitation, Hospital of Southern Norway, 4838 Arendal, Norway, [10]Department of Pediatrics, Hospital of Southern Norway, 4838 Arendal, Norway, [11]Division of Genetics & Metabolism, Phoenix Children's Medical Group, Phoenix, AZ 85016, USA, [12]Center for Mendelian Genomics and Program in Medical and Population Genetics, Broad Institute of MIT and Harvard, Cambridge, MA 02142, USA, [13]Invitae Corporation, San Francisco, CA 94103, USA, [14]Senckenberg Centre for Human Genetics, 60314 Frankfurt/Main, Germany, [15]Institute of Human Genetics, University Hospital of Cologne, 50931 Cologne, Germany, [16]Institute of Human Genetics, University Medical Center Mainz, 55131 Mainz, Germany and [17]Department of Pediatrics, Ann & Robert H. Lurie Children's Hospital of Chicago, Northwestern University Feinberg School of Medicine, Chicago, IL 60611, USA

*To whom correspondence should be addressed at: Center for Experimental Medicine, Institute for Cellular and Integrative Physiology, University Hospital Hamburg-Eppendorf, Martinistr. 52, 20246 Hamburg, Germany. Tel: +49 (0) 40 741058638; Fax: +49 (0) 40 741059127; Email: r.baehring@uke.de

Abstract

Here, we report on six unrelated individuals, all presenting with early-onset global developmental delay, associated with impaired motor, speech and cognitive development, partly with developmental epileptic encephalopathy and physical dysmorphisms. All individuals carry heterozygous missense variants of *KCND2*, which encodes the voltage-gated potassium (Kv) channel α-subunit Kv4.2. The amino acid substitutions associated with the variants, p.(Glu323Lys) (E323K), p.(Pro403Ala) (P403A), p.(Val404Leu) (V404L) and p.(Val404Met) (V404M), affect sites known to be critical for channel gating. To unravel their

Received: February 26, 2021. **Revised:** July 6, 2021. **Accepted:** July 7, 2021

likely pathogenicity, recombinant mutant channels were studied in the absence and presence of auxiliary β-subunits under two-electrode voltage clamp in *Xenopus* oocytes. All channel mutants exhibited slowed and incomplete macroscopic inactivation, and the P403A variant in addition slowed activation. Co-expression of KChIP2 or DPP6 augmented the functional expression of both wild-type and mutant channels; however, the auxiliary β-subunit-mediated gating modifications differed from wild type and among mutants. To simulate the putative setting in the affected individuals, heteromeric Kv4.2 channels (wild type + mutant) were studied as ternary complexes (containing both KChIP2 and DPP6). In the heteromeric ternary configuration, the E323K variant exhibited only marginal functional alterations compared to homomeric wild-type ternary, compatible with mild loss-of-function. By contrast, the P403A, V404L and V404M variants displayed strong gating impairment in the heteromeric ternary configuration, compatible with loss-of-function or gain-of-function. Our results support the etiological involvement of Kv4.2 channel gating impairment in early-onset monogenic global developmental delay. In addition, they suggest that gain-of-function mechanisms associated with a substitution of V404 increase epileptic seizure susceptibility.

Introduction

Global developmental delay (GDD) is defined as a significant delay in two or more developmental domains including (a) gross or fine motor behavior, (b) speech and language, (c) cognition, (d) personal–social skills and (e) activities of daily living, affecting children under the age of 5 (1,2). With a prevalence of 1–3%, GDD represents one of the most common conditions observed in pediatrics (3–5). GDD is frequently caused by heterozygous *de novo* variants in developmental genes, particularly those expressed in neurons, and thus often associates with brain malformations and/or altered neuronal functioning (6). The latter may include changes in excitability and discharge behavior, known to be directly controlled by ion channels in neuronal cell membranes, first and foremost voltage-dependent potassium (Kv) channels. The Kv channels are encoded by a large gene superfamily with 12 subfamily members (7) (see also Supplementary Material, Fig. S1). The specific role of a particular Kv channel subtype in cellular neurophysiology is determined by its relative expression level and subcellular localization, as well as its voltage dependencies and kinetics of activation and inactivation. Members of the Kv4 subfamily, especially Kv4.2, mediate a subthreshold-activating somatodendritic A-type (i.e. rapidly activating and inactivating) current (I_{SA}) (8). The Kv4 channel-mediated I_{SA} is involved in many aspects of cellular neurophysiology, including action potential repolarization and frequency-dependent spike broadening (9), control of dendritic excitation and action potential back-propagation (10), as well as synaptic filtering (11) and synaptic plasticity (12). Notably, the Kv4 channel-mediated I_{SA} is downregulated in animal models of cortical malformations and epilepsy (13–19).

Like all members of the Kv superfamily, Kv4 channel α-subunits consist of six transmembrane segments (S1–S6), with cytoplasmic N- and C-termini and a re-entrant loop between S5 and S6, which harbors the potassium selectivity filter sequence (Fig. 1A). The α-subunits tetramerize to form functional channels. Within a tetramer, the S1–S4 helices (particularly the positively charged amino acid residues in S4) function as voltage sensors residing in the channel periphery. The S5 and S6 helices surround the central ion conduction pathway with the intertwined and flexible distal S6 segments functioning as the cytoplasmic gate (20). Mechanical coupling of the voltage sensors to the cytoplasmic gate, which allows for voltage-dependent channel opening and closing, is provided by mutual interactions between residues in the S4S5 linker and the distal S6 segment (21,22) (Fig. 1). In Kv4 channels, these residues are also critically involved in inactivation (23,24).

Native Kv4 channels are thought to form ternary complexes with auxiliary Kv channel-interacting proteins (KChIPs) and/or dipeptidyl peptidase-related proteins (DPPs) (25). In heterologous expression systems, both KChIPs and DPPs increase Kv4 channel surface expression (26–30). Moreover, both auxiliary β-subunits modulate Kv4 channel gating in a specific manner: KChIPs cause a slowing of macroscopic inactivation and a positive shift in the voltage dependence of steady-state inactivation (26,27,29,31), whereas DPPs cause an acceleration of macroscopic inactivation and a negative shift in the voltage dependencies of both activation and steady-state inactivation (28,30,32). Both auxiliary β-subunits accelerate the recovery from inactivation (26–32). These specific modifications have to be taken into account when evaluating Kv4 channel function in a native setting and when considering the likely pathogenicity of mutant variants.

Kv4 channels are encoded by three different genes (*KCND1–3*; Supplementary Material, Fig. S1) (33). Here, we report on six unrelated individuals with early-onset GDD and heterozygous missense variants of *KCND2*. The associated amino acid substitutions, p.(Glu323Lys) (E323K), p.(Pro403Ala) (P403A, two individuals), p.(Val404Leu) (V404L, two individuals) and p.(Val404Met) (V404M), affect residues, which are involved in controlling the cytoplasmic gate. Functional testing of mutant variants revealed distinct perturbations of channel gating, which are compatible with both a partial loss-of-function (LOF) and gain-of-function (GOF). Our findings strongly implicate Kv4.2 channel gating impairment in the etiology of early-onset GDD and suggest that substituting V404 increases epileptic seizure susceptibility.

Results

Clinical and genomic data

In this study, we report on six individuals (cases 1–6) from six unrelated families with diverse ethnic background, all affected by early-onset GDD of distinct severity. In each case, first symptoms were noted within the first 6 months of life (Table 1 and Supplementary Material, Clinical Reports). All six individuals presented with significant delays in motor, speech and cognitive development. Five individuals exhibited muscle hypotonia (cases 2–6) and three individuals had seizures (cases 4–6). Three individuals showed visual impairments (cases 2, 3 and 5), presenting with either progressively declining vision and a strong evidence for rod/cone dystrophy (case 2), cortical visual impairment combined with intermittent lateral nystagmus (case 3) or lack of fixation and strabismus associated with hypomyelination of the visual tract (case 5). Mild physical dysmorphisms were observed for two individuals (cases 2 and 6), including either a tall forehead, small mouth, high arched palate, short and small nose, bilateral epicanthal folds and mild two-three

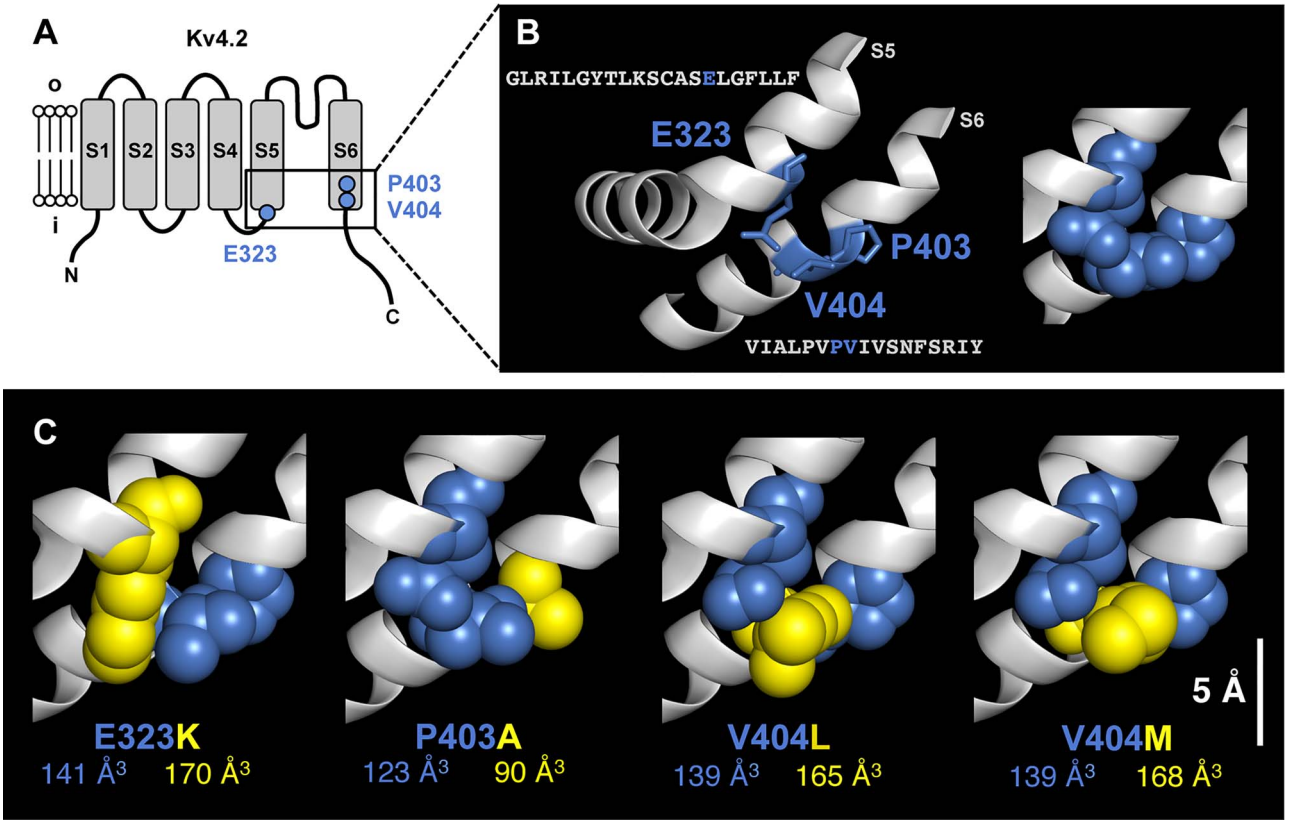

Figure 1. Kv4.2 α-subunit and amino acid substitutions. (**A**) Scheme of membrane topology of the Kv4.2 α-subunit containing six transmembrane segments (S1–S6) with a re-entrant loop between S5 and S6 (o: outside; i: inside, with N- and C-terminus). Amino acid residues in the S4S5 linker and the distal S6 segment affected by the reported *KCND2* variants are indicated (blue circles). (**B**) Topology prediction of S4S5 linker and distal S6 segment. Corresponding Kv4.2 amino acid sequences are shown; protein backbone depicted as ribbon diagram; side chains of E323, P403 and V404 depicted in stick mode (left) and as CPK models (right). (**C**) Mutation-associated amino acid substitutions were simulated with the most likely backbone-dependent rotamer orientation; CPK models of native and novel amino acid side chains shown in blue and yellow, respectively; mean side chain volumes indicated.

toe syndactyly (case 2), or deep set almond shaped eyes, pointed chin, prominent brow ridge, small nose, large anteriorly rotated ears and tall forehead (case 6). Finally, in two individuals, brain malformations were detected: pronounced cortical frontotemporal brain atrophy with mild expansion of inner liquor spaces (case 5), or decrease in both periventricular and deep white matter combined with prominent ventricles (case 6). Noteworthy, in three individuals (cases 4–6), a developmental epileptic encephalopathy was diagnosed (see Supplementary Material, Clinical Reports for electroencephalographical details and pharmacological treatment). One of these individuals (case 5) died at 21 years of age, the cause of death being unknown.

Utilizing next-generation sequencing, we identified different heterozygous missense variants of *KCND2* (NM_012281.3) in the reported individuals. In each case, the *KCND2* variant represented the only or most convincingly disease-related gene variant (Supplementary Material, Clinical Reports). In four individuals (cases 3–6), a *de novo* origin of the variant was confirmed. For the remaining two cases (cases 1 and 2), the origin of the *KCND2* variant could not be determined owing to the lack of parental DNA specimens. Two individuals (cases 2 and 3) carry the same gene variant, and in two other individuals (cases 4 and 5), two distinct nucleotide exchanges result in the same amino acid substitution. Thus, we are dealing with four different amino acid substitutions: c.967G>A;p.(Glu323Lys) (case 1), c.1207C>G;p.(Pro403Ala) (cases 2 and 3), c.1210G>T;p.(Val404Leu) (case 4), c.1210G>C;p.(Val404Leu) (case 5) and c.1210G>A;p.(Val404Met) (case 6). Noteworthy, the three individuals diagnosed with developmental epileptic encephalopathy (cases 4–6) all harbor Val404 substitutions (Table 1). None of the newly identified *KCND2* variants is listed in the public gnomAD database (https://gnomad.broadinstitute.org/; gnomAD v2.1.1, GRCh37/hg19). Applied bioinformatics programs predicting the functional relevance of variants (CADD, REVEL, M-CAP, SIFT, Polyphen 2) uniformly predict a deleterious effect on protein function. While the 1210G>A;p.(Val404Met) variant has been previously identified in monozygotic twins affected by severe, intractable seizures and autism (34), the remaining variants are novel. All identified *KCND2* variants affect highly conserved Kv4.2 amino acid residues (Supplementary Material, Fig. S1) critical for channel gating Figure 1; (21–23,35), thus providing initial evidence for their likely pathogenicity. For simplicity, amino acid substitutions and corresponding mutant Kv4.2 channels will be referred to as E323K, P403A, V404L and V404M, respectively.

Functional characterization of mutant Kv4.2 channels in the absence and presence of auxiliary subunits

The four different amino acid substitutions affect sites, which are involved in the operation of the cytoplasmic gate (Fig. 1) (21–23,35). To assess the hypothesis that all four amino acid substitutions critically influence gating with a detrimental impact on normal channel function, recombinant wild-type (WT) and mutant Kv4.2 channels were expressed alone or together with

Table 1. Genetic and clinical features of individuals carrying missense mutations in *KCND2*

case	1	2	3	4	5	6
Genomic position GRCh38/hg38	chr7:120275599	chr7:120732994	chr7:120732994	chr7:120732997	chr7:120732997	chr7:120732997
Mutation in cDNA NM_012281.2	c.967G>A	c.1207C>G	c.1207C>G	c.1210G>T	c.1210G>C	c.1210G>A
Amino acid alteration NP_036413	p.Glu323Lys (E323K)	p.Pro403Ala (P403A)	p.Pro403Ala (P403A)	p.Val404Leu (V404L)	p.Val404Leu (V404L)	p.Val404Met (V404M)
Inheritance	n.d.	n.d.	*de novo*	*de novo*	*de novo*	*de novo*
Zygosity	Heterozygous	Heterozygous	Heterozygous	Heterozygous	Heterozygous	Heterozygous
gnomAD alleles (v2.1.1)[a]	0	0	0	0	0	0
Sex	Male	Female	Female	Male	Female	Female
Ethnicity	Caucasian	Caucasian	Native American	Caucasian	Caucasian	Latin American
Age at first symptoms	From birth	5 months	<1 year	6 months	3 months	3 months
Current age	13 years	10 years	11 years	2 years 6 months	Deceased at the age of 21 years	3 years 6 months
GDD	+	+	+	+	+	+
Motor behavior	+	+	+	+	+	+
Speech/language	+	+	+	+	+	+
Cognition	+	+	+	+	+	+
Personal-social	+	n.d.	n.d.	+	+	−
Muscle hypotonia	−	+	+	+	+	+
Seizures	−	−	−	+	+	+
Encephalopathy	n.d.	+	n.d.	+	+	+
Autism	−	−	−	+	n.d.	−
Visual impairment	−	+	+	−	+	−
Brain malformations	n.d.	−	−	−	+	+
Physical dysmorphism	−	+	−	−	−	+

+, feature present; −, feature absent; n.d., no data.
[a]More than 250.000 alleles analysed.

auxiliary β-subunits in *Xenopus* oocytes and functionally characterized under two-electrode voltage clamp (see Materials and Methods).

Kv4.2 WT and all tested mutants mediated outward currents in response to depolarizing voltage pulses, albeit with extremely small amplitudes for E323K and P403A. Like Kv4.2 WT, all mutants exhibited increased current amplitudes when co-expressed with either KChIP2 or DPP6, although this effect was moderate for E323K and especially for P403A (Fig. 2A and B; Supplementary Material, Table S1). Thus, the mutant Kv4.2 proteins are able to form functional channels and interact with both types of auxiliary β-subunits. For V404L and V404M, the voltage dependence of activation was similar to Kv4.2 WT, but E323K and P403A showed an apparent positive shift of ∼10 and ∼60 mV, respectively (Fig. 2C; Supplementary Material, Table S1). For both WT and mutant channels, the voltage dependence of activation was steepened by auxiliary β-subunit co-expression with a negative shift caused by DPP6 (Fig. 2C; Supplementary Material, Table S1).

For all tested mutants, the time course of the currents differed from Kv4.2 WT (Fig. 3). Notably, P403A mediated extremely slow activating currents, which did not reach a peak during the applied test pulse, whereas the other mutants showed virtually unaltered activation kinetics. However, the initial current decay kinetics was slowed, and the remaining current at the end of the test pulse was increased for these mutants (Fig. 3; Supplementary Material, Table S2). For P403A, KChIP2 co-expression caused an acceleration of activation kinetics, so that the currents reached a peak during the test pulse, thereby unveiling slow decay kinetics. By contrast, DPP6 did not affect the activation kinetics of P403A, and current decay was only apparent with longer test pulses (Supplementary Material, Fig. S2). The finding that P403A-mediated currents decayed in response to prolonged depolarization, albeit extremely slowly, indicates that, similar to the other mutants, P403A undergoes inactivation. Macroscopic inactivation of the other mutants was modified by KChIP2, but the effects differed from Kv4.2 WT. For E323K, KChIP2 co-expression caused an acceleration rather than a slowing, whereas for both V404L and V404M, KChIP2 co-expression caused an extreme slowing of current decay. DPP6 caused the typical acceleration of current decay for E323K, V404L and V404M (Fig. 3; Supplementary Material, Table S2).

Next, the voltage dependence of steady-state inactivation and the kinetics of recovery from inactivation were studied (Fig. 4). Compared to Kv4.2 WT, the voltage dependence of steady-state inactivation was negatively shifted for E323K and V404M, and for all examined mutants, the amount of inactivation at the most depolarized voltage tested was incomplete. KChIP2 caused the typical positive shift in the voltage dependence of steady-state inactivation for E323K and V404L, but not for V404M, whereas DPP6 caused the typical negative shift for V404L and V404M, but not for E323K (Fig. 4A; Supplementary Material, Table S2). The recovery from inactivation was accelerated compared to Kv4.2 WT for E323K but slowed for V404L and V404M. KChIP2 caused the typical acceleration of recovery kinetics for all of these mutants. Notably, the typical acceleration of recovery kinetics mediated by DPP6 was seen for E323K, whereas the recovery kinetics of V404L and V404M remained virtually unaffected by DPP6 (Fig. 4B; Supplementary Material, Table S2). For P403A, the analysis of the voltage dependence of steady-state inactivation and recovery kinetics was restricted to the data obtained in the presence of

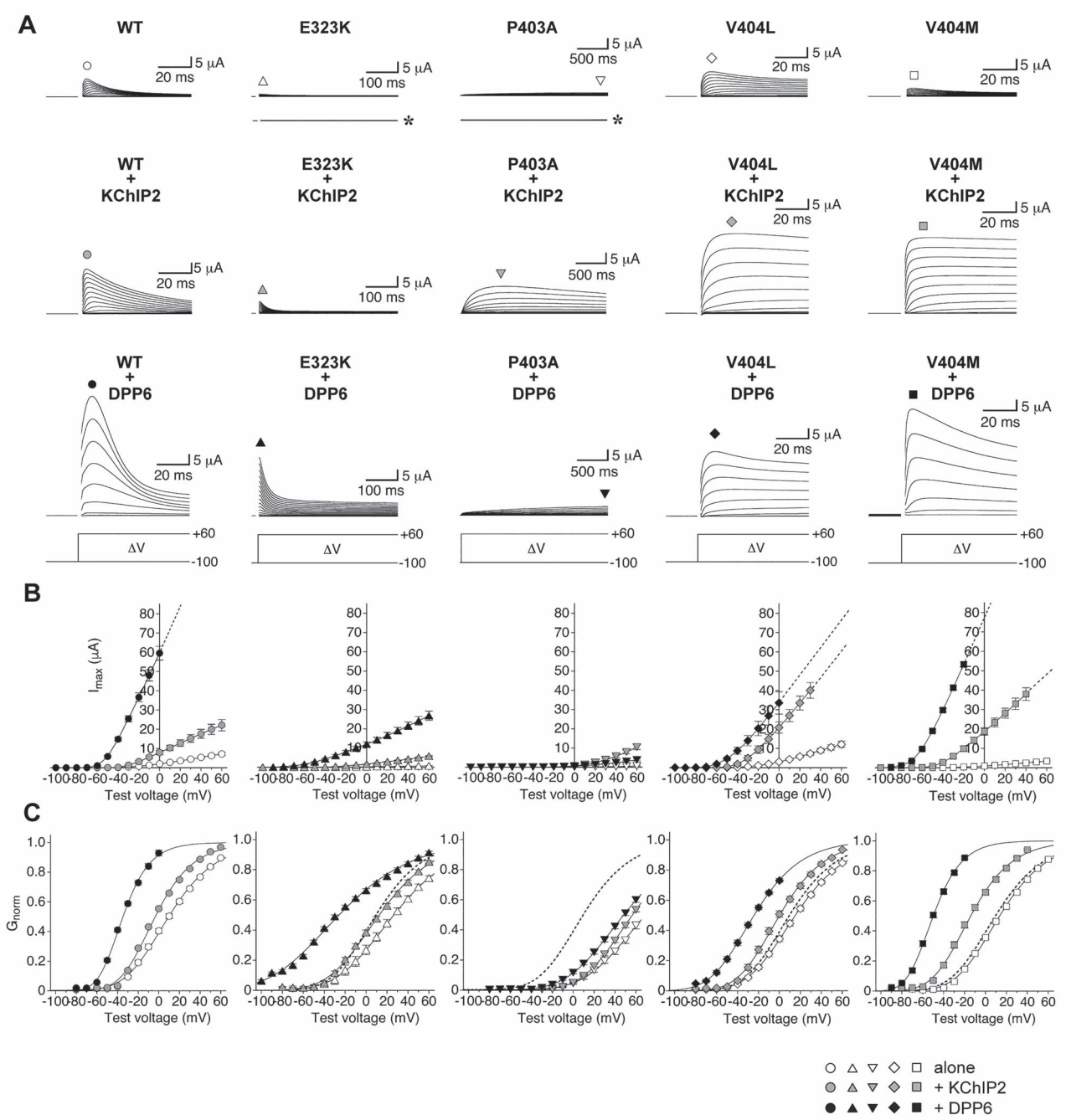

Figure 2. Voltage-dependent activation of Kv4.2 channel variants. Kv4.2 channels were expressed in *Xenopus* oocytes, either alone or in combination with KChIP2 or DPP6, and macroscopic currents were recorded under two-electrode voltage clamp. (**A**) Current families obtained 2 days after cRNA injection with pulses from −100 mV to different test voltages between −100 and +60 mV (ΔV: 10 mV increments). Currents are shown for WT, E323K, P403A, V404L and V404M expressed alone, with KChIP2 and with DPP6 (capacitive transients omitted and current traces not shown in full length). Note the different time scales and extremely small current amplitudes for E323K and P403A alone (asterisks: water-injected controls from the same batch of oocytes). (**B**) Current amplitudes (measured at the time points indicated by the symbols in (A) plotted against test voltage for WT (circles), E323K (triangles), P403A (inverted triangles), V404L (diamonds) and V404M (squares). Data obtained with non-reliable voltage-clamp were omitted; dotted lines: extrapolation drawn by eye. (**C**) Voltage dependence of activation; cord conductance values were used to generate normalized conductance (G_{norm})-voltage plots for Boltzmann analysis (23,38). Dotted Boltzmann curves: Kv4.2 WT expressed alone. Empty symbols: channels expressed alone; grey and black symbols: co-expression of KChIP2 and DPP6, respectively.

auxiliary β-subunits. A comparison of the voltage dependencies of steady-state inactivation for P403A in the presence of KChIP2 or DPP6 with corresponding WT data suggested that the P403A substitution also caused inactivation to be incomplete at the most depolarized voltage tested. Remarkably, the voltage dependence of steady-state inactivation adopted a biphasic shape for P403A + KChIP2, which persisted if KChIP2 was massively overexpressed (data not shown). A comparison of the recovery kinetics obtained for P403A in the presence of KChIP2 or DPP6 with corresponding WT data suggested that the P403A

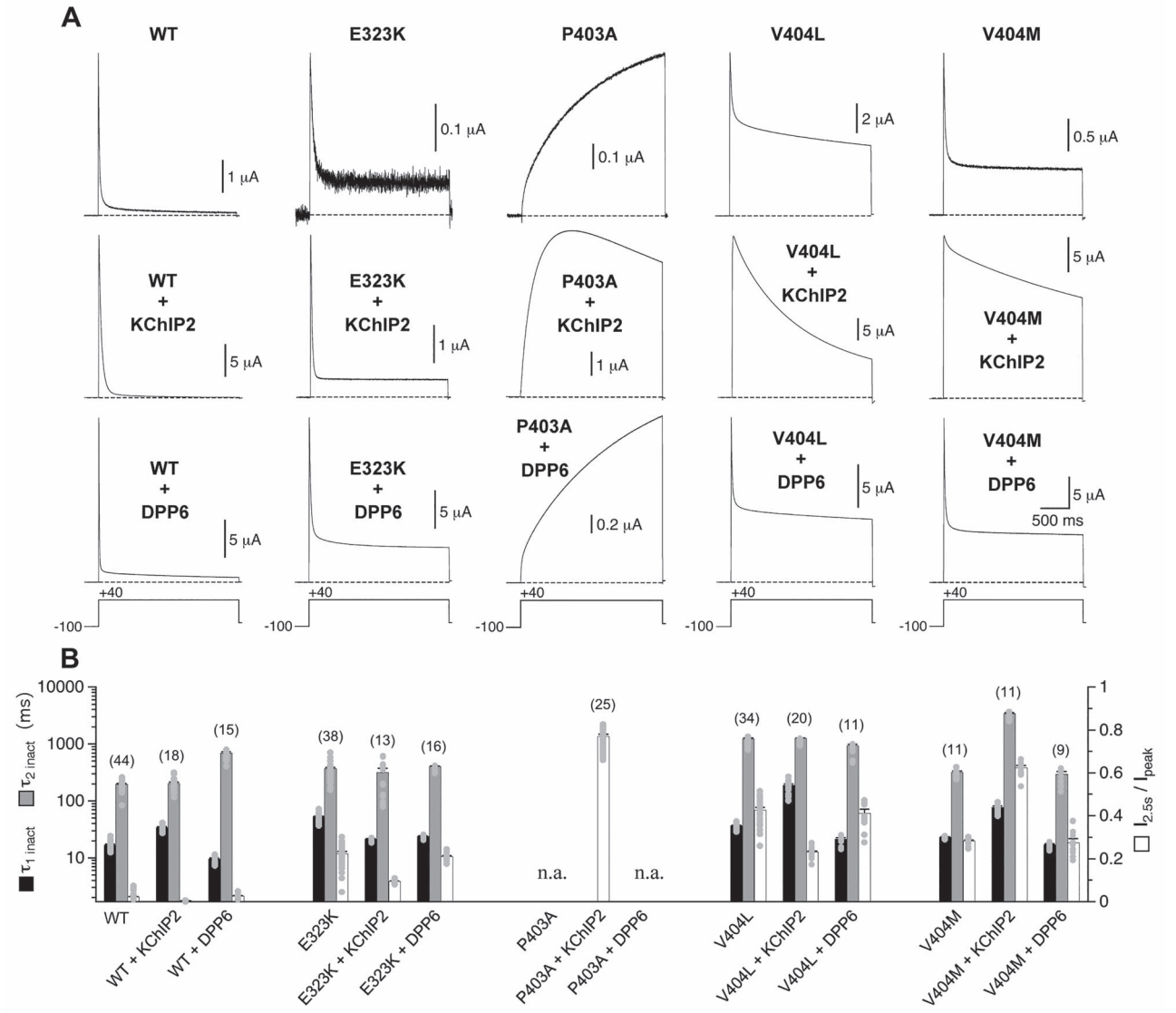

Figure 3. Kinetics of macroscopic inactivation. Modulation of Kv4.2 channel-mediated macroscopic current decay by the mutations and by auxiliary β-subunit co-expression. (**A**) Currents during a 2.5 s test pulse to +40 mV recorded 1–3 days after cRNA injection from oocytes expressing Kv4.2 WT, E323K, P403A, V404L or V404M in the absence of auxiliary β-subunits, together with KChIP2, or together with DPP6 (dotted line: zero current). Note that currents mediated by P403A alone and P403A + DPP6 do not reach a maximum during the test pulse. Note also the incomplete current decay for the other mutant channels and the pronounced slowing of current decay for V404L and V404M in the presence of KChIP2. (**B**) Bar graph showing macroscopic inactivation quantified by the time constants obtained with double-exponential fitting (black and grey bars) and the relative current at the end of the test pulse ($I_{2.5s}/I_{peak}$, empty bars); numbers of oocytes (n) indicated; n.a.: not analysed.

substitution caused a slowing of recovery kinetics (Fig. 4A and B; Supplementary Material, Table S2).

Heteromeric assembly of WT and mutant channel subunits and ternary complex formation

All *KCND2* variants reported herein are monoallelic, compatible with an autosomal dominant mode of inheritance. Thus, we tested whether and how mutant co-expression influences the currents mediated by Kv4.2 WT (Supplementary Material, Fig. S3). For E323K, V404L and V404M the co-expression with WT resulted in currents with intermediate characteristics. Titration effects were particularly obvious for the relative current at the end of the test pulse, albeit with apparently different cRNA dose dependencies for the individual mutants. P403A co-expression at equal cRNA amounts led to an almost complete suppression of the fast macroscopic inactivation of Kv4.2 WT, while a 4-fold excess of mutant cRNA gave rise to slowly activating currents with no peak during the applied test pulse (Supplementary Material, Fig. S3, Supplementary Material, Tables S1 and S2). These results substantially differed from the theoretical sum of currents as predicted for two separate homomeric WT and P403A channel populations (Supplementary Material, Fig. S3), strongly suggesting WT and mutant Kv4.2 α-subunit co-assembly.

Native Kv4 channels are thought to form ternary complexes with KChIPs and DPPs (25). Therefore, heteromeric (WT + mutant) Kv4.2 channels were simultaneously co-expressed with both KChIP2 and DPP6 to simulate the putative setting in the affected individuals (see Materials and Methods). Properties of WT + mutant ternary channels were compared

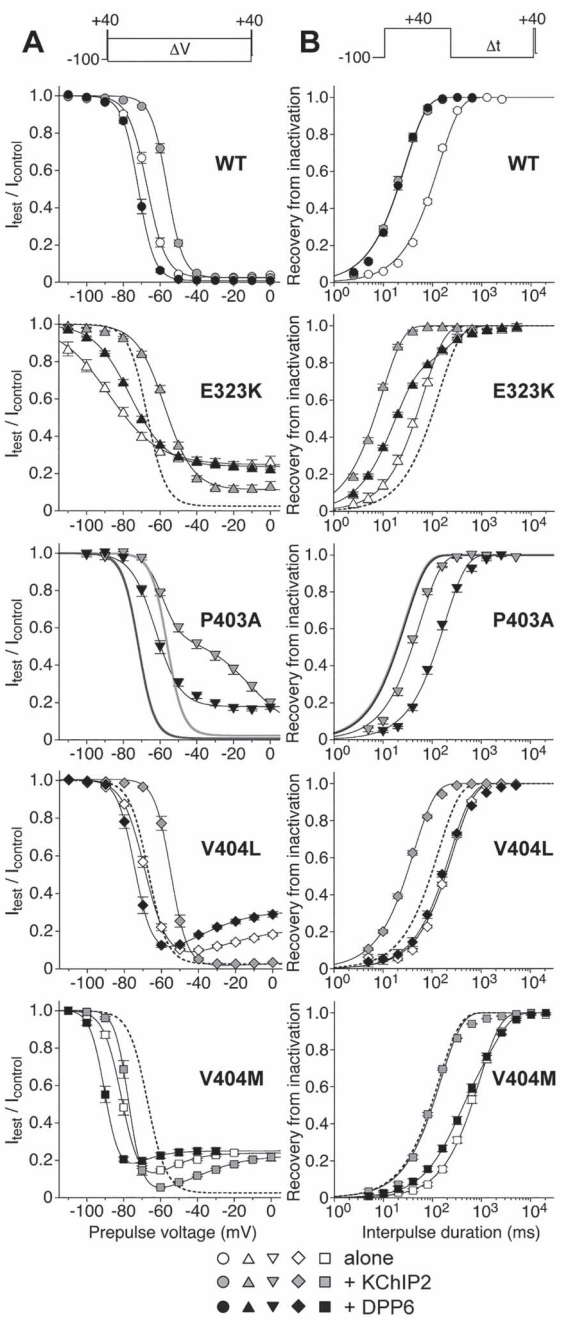

Figure 4. Voltage dependence of steady-state inactivation and recovery kinetics. (**A**) Voltage dependence of steady-state inactivation for Kv4.2 WT and mutant channels was measured using a double-pulse protocol with a constant interpulse length (10 s) and interpulse voltages varying between −110 and 0 mV (ΔV: 10 mV increments, see inset). Relative current amplitudes obtained with the second pulse were plotted against prepulse voltage, and data were fitted with a single or, if necessary, the sum of two Boltzmann functions. Note the biphasic voltage dependencies for P403A + KChIP2, V404L alone and with DPP6, and V404M both in the absence and presence of auxiliary β-subunits. (**B**) Recovery from inactivation was measured using a double-pulse protocol with an interpulse voltage of −100 mV and interpulse durations of ≥5 ms (Δt factor = 2, see inset). Relative current amplitudes obtained with the second pulse were plotted against interpulse interval, and the data were fitted with a single- or, if necessary, a double-exponential function. Note the slowed recovery kinetics compared to WT for all mutants except E323K and the moderate effect of DPP6 on the recovery kinetics of V404L and V404M. Empty symbols: channels expressed alone; grey and black

with those of homomeric WT ternary. Averaged peak current amplitudes were similar for WT ternary, WT + V404L ternary and WT + V404M ternary, whereas WT + E323K ternary and WT + P403A ternary mediated smaller currents (Fig. 5A–C; Supplementary Material, Table S1). The voltage dependence of activation was indistinguishable from homomeric WT ternary for WT + E323K ternary, shifted positive for WT + P403A ternary and negative for both WT + V404L ternary and WT + V404M ternary (Fig. 5D; Supplementary Material, Table S1). Studying the inactivation properties of WT + mutant ternary channels revealed that their macroscopic inactivation kinetics diverged to different degrees from homomeric WT ternary. WT + E323K ternary-mediated currents were very similar to those of homomeric WT ternary, except that macroscopic inactivation was not quite complete. However, the other mutants exerted a prominent effect on macroscopic inactivation, even in the heteromeric ternary configuration. Current decay was slowed, and the remaining current at the end of the test pulse was increased. In the heteromeric ternary configuration, the impact of V404L was stronger than that of V404M, and P403A exerted the strongest effect on macroscopic inactivation (Fig. 5E and F; Supplementary Material, Table S2). As a measure of LOF or GOF, the combined mutant effects on current amplitude and decay kinetics were quantified by calculating the integral below the respective current traces (Fig. 5G; see Supplementary Material, Table S1 and Discussion). Concerning the voltage dependence of steady-state inactivation, WT + V404L ternary and WT + V404M ternary channels were virtually identical to homomeric WT ternary, whereas WT + E323K ternary and WT + P403A ternary inactivated at slightly more depolarized voltages (not significant for WT + E323K ternary), and steady-state inactivation was incomplete for WT + P403A ternary (Fig. 5H). The kinetics of recovery from inactivation resembled homomeric WT ternary for WT + E323K ternary and WT + V404M ternary, whereas WT + P403A ternary and WT + V404L ternary recovered from inactivation more slowly (Fig. 5I; Supplementary Material, Table S2).

Ternary Kv4.2 channel analysis was extended to the kinetics of activation and deactivation (Fig. 6). The slow activation kinetics caused by the P403A substitution (see Fig. 3A) was still apparent in the heteromeric ternary configuration and correlated with the positively shifted voltage dependence of activation for WT + P403A ternary (see Fig. 5D). The other variants did not significantly influence activation kinetics in the heteromeric ternary configuration (Fig. 6A and B; Supplementary Material, Table S1). Finally, the kinetics of channel closure was examined. Remarkably, all heteromeric WT + mutant ternary channels showed slower deactivation kinetics than homomeric WT ternary. The effect was moderate for WT + E323K ternary, stronger for WT + V404M ternary, and most prominent for WT + V404L ternary and WT + P403A ternary (Fig. 6C and D; Supplementary Material, Table S1). Taken together, these data show that in the heteromeric ternary configuration some forms of gating impairment become less apparent, while others persist. The latter are compatible with both LOF and GOF. The positively shifted voltage dependence and slow kinetics of activation caused by P403A (partial LOF) and the extremely slow macroscopic inactivation and deactivation kinetics caused by both P403A and V404L (GOF) should be especially noted in this context (Supplementary Material, Tables S1 and S2).

Kv4.2 channels inactivate more readily from pre-open closed states than from the open state (36). Since this preferential closed-state inactivation (CSI) plays an important role in

dendritic excitation and synaptic plasticity, and since the amino acid substitutions identified herein affect sites, which are critically involved in gating, we examined whether CSI is still the predominant inactivation pathway in the heteromeric WT + mutant ternary channels. To that end, we tested for kinetic features of inactivation indicative of a significant contribution of open-state inactivation (Supplementary Material, Fig. S4). However, we neither found an obvious decline of inactivation time constants with increasing depolarization (Supplementary Material, Fig. S4A), nor did the rate of inactivation match open probability during moderate depolarization (Supplementary Material, Fig. S4B). Based on these tests, which supported the presence of preferential CSI in both homomeric WT ternary and heteromeric WT + mutant ternary channels, we finally determined the kinetics of CSI at a voltage of −60 mV, expected to induce negligible open probability. We found that CSI on and off rates were specifically modified in all WT + mutant ternary channels, except for WT + E323K ternary (Supplementary Material, Fig. S4C). The structure–function relationship of the mutant impact on Kv4.2 channel CSI, the putative pathogenic effects of Kv4.2 channel LOF and GOF and the clinical phenotypes associated with Kv4 channel dysfunction will be discussed.

Discussion

We have studied recombinant mutant Kv4.2 channels with single amino acid substitutions, corresponding to heterozygous *KCND2* missense variants found in a cohort of infants presenting with GDD. The occurrence of two identical and two similar *KCND2* variants and the independent recurrence of a previously reported variant (34) within our study identify the respective codons as putative disease-associated mutational 'hotspots'. Combined with our functional data, this corroborates the particular importance of the S4S5 linker and the distal S6 segment for accurate Kv4.2 channel function. By testing the mutant Kv4.2 channels in a native setting, we provide strong evidence that the identified *KCND2* variants lead to a syndromic neurodevelopmental disorder, which includes impaired motor development, speech and cognition, as well as possible epileptic seizures, brain malformations and physical dysmorphisms.

Mutation-associated impairment of channel gating

All *KCND2* variants reported herein affect Kv4.2 amino acid residues in highly conserved domains, which are directly involved in operating the cytoplasmic gate. Therefore, each of the four amino acid substitutions examined, E323K, P403A, V404L and V404M, in itself profoundly alters Kv4.2 channel gating. P403, which is altered in cases 2 and 3 (Table 1), represents the second proline of a PXP motif, highly conserved in Kv1–Kv4 channels (see Supplementary Material, Fig. S1). Our study demonstrates a strong positive shift in the voltage dependence of activation and extremely slow activation kinetics for P403A. These findings support the general idea that the PXP motif allows the S6 helix to bend, which is critical for opening and closing of the cytoplasmic gate (20). Moreover, our data obtained in the presence of auxiliary β-subunits suggest that the P403A substitution *per se* attenuates Kv4.2 channel inactivation, supporting the notion that S6 motion is involved in Kv4.2 channel inactivation (23).

Intriguingly, substituting the valine residue directly following the PXP motif (V404L in cases 4 and 5, and V404M in case 6) leaves activation kinetics more or less unaffected, but critically influences Kv4.2 channel inactivation. In V404L and V404M inactivation is attenuated at depolarized voltages. In fact, both mutants show a biphasic voltage dependence of inactivation with typical U-type features (i.e. inactivation is strongest at intermediate voltages), which is a most obvious indicator of preferential CSI (36). Notably, this feature is not evident in Kv4.2 WT, because these channels normally accumulate in closed-inactivated states at all relevant membrane voltages (23,36). Yet, U-type features have been described previously for certain Kv4.2 mutants including V404M (23,35). The U-type features observed herein for both V404L and V404M can be explained by a strong impairment of inactivation once these channels have opened, presumably due to their slowed channel closure, as suggested previously for V404M (35; see also Fig. 6) and for a similar mutant of Kv4.1 (24). It is widely accepted that Kv4 channels need to close in order to fully inactivate (36); however, the actual mechanism of Kv4 channel CSI is still unknown. It has been proposed that the S4S5 linker and the distal S6 segment may lose their mutual physical contact during Kv4 channel CSI (23). This view is challenged by the finding that, despite the larger side chain volume of methionine (168 Å^3) compared to valine (139 Å^3; Fig. 1C) (37), which may actually favor physical contact, CSI is enhanced (i.e. the voltage dependence of inactivation is negatively shifted) for V404M (see also Fig. 4A) (35). However, it should be noted that a previously studied V404A mutant with a reduced side chain volume of 90 Å^3 also displayed a negative shift in the voltage dependence of inactivation (23), even larger than that observed for V404M in the present study. Moreover, our results show that, despite the similar side chain volumes of methionine (168 Å^3) and leucine (165 Å^3; Fig. 1C) (37), the effects of V404M and V404L are distinct. Intriguingly, in one of our individuals (case 1) E323, a critical thermodynamic coupling partner of V404 (23,38) is affected. In the E323K mutant, not only side chain volume, which is increased from 141 to 170 Å^3 (Fig. 1C) (37), but also the charge of the side chain (from negative to positive) is modified. As a consequence of the E323K substitution, the voltage dependence of inactivation becomes more negative but shallow, and inactivation is incomplete at depolarized voltages. It is remarkable that reducing the volume (from 141 to 90 Å^3) and neutralizing the charge of the side chain at this position (E323A) also caused a negative shift (23), whereas a highly conservative amino acid substitution (E323D) apparently caused a positive shift in the voltage dependence of inactivation (35). Taken together, these findings suggest that, in addition to side chain volume and charge, other structural features critically determine Kv4.2 channel CSI. Also, in addition to E323 and V404, other amino acid residues, located outside the mutational 'hotspots' identified herein (38), may be involved in the dynamic coupling between the S4S5 linker and the distal S6 segment during the process of Kv4.2 channel CSI. Obviously, the structure–function relationship of Kv4.2 channel CSI, although already studied in some detail (35,36,38,39), has not been resolved with sufficient clarity and requires further examination in a different context. Of central importance for the present study, although none of the

symbols: co-expression of KChIP2 and DPP6, respectively; dotted fitting curves: WT expressed alone. Since the voltage dependence of steady-state inactivation and recovery kinetics could not be measured for P403A alone, the fitting curves for WT + KChIP2 and WT + DPP6 (solid light and dark grey lines without symbols, respectively) are shown as reference for P403A + KChIP2 and P403A + DPP6.

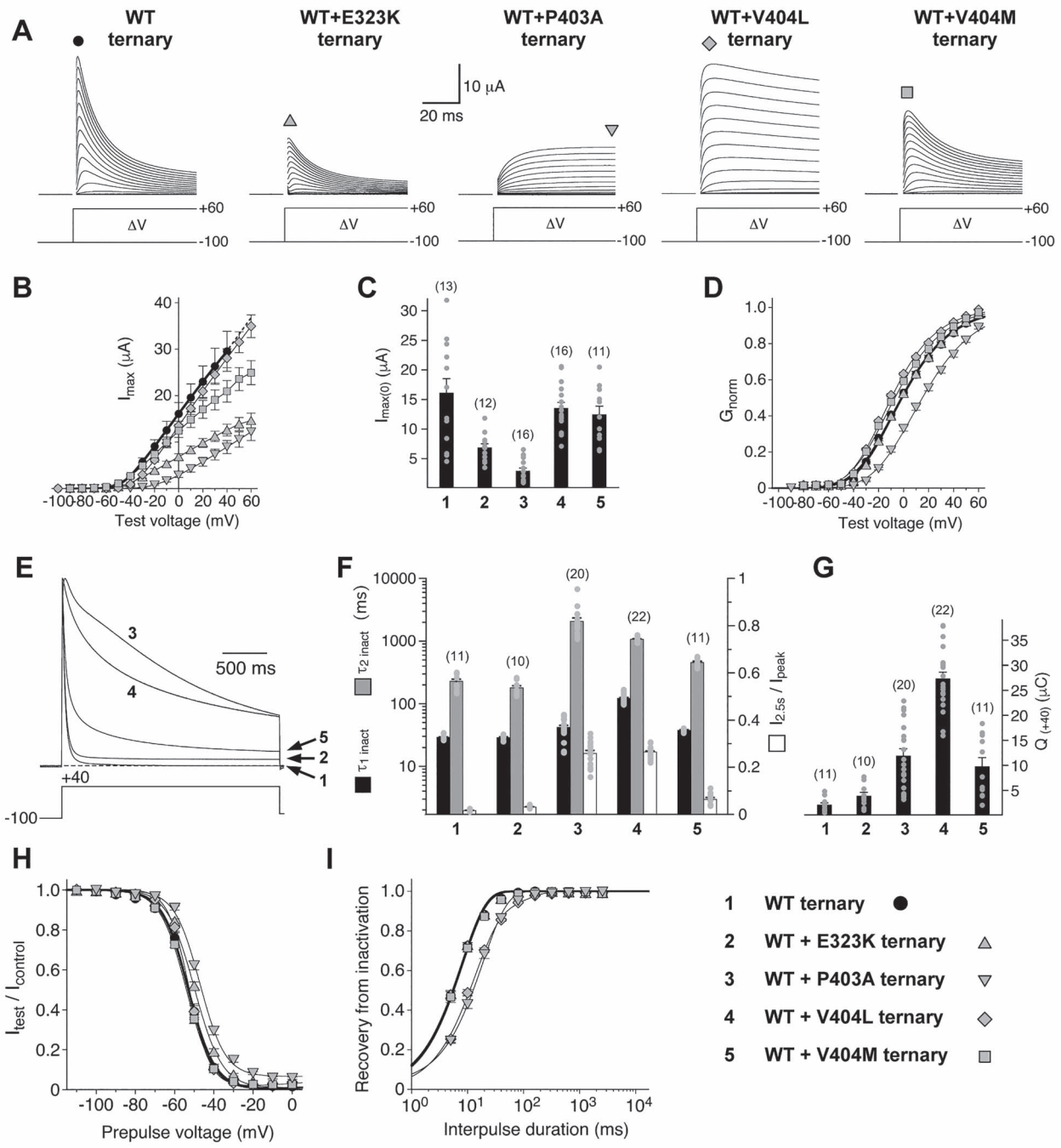

Figure 5. Activation and inactivation of Kv4.2 WT and heteromeric WT + mutant ternary complexes. Homomeric WT and heteromeric WT + mutant Kv4.2 channels were studied in a ternary configuration with KChIP2 and DPP6. The data are marked by numbers and symbols: (1) WT ternary, circles; (2) WT + E323K ternary, triangles; (3) WT + P403A ternary, inverted triangles; (4) WT + V404L ternary, diamonds; (5) WT + V404M ternary, squares (see also inset on the lower right). (**A**) Current families obtained 1 day after cRNA injection. (**B**) Current amplitudes (measured at the time points indicated by the symbols in (A) plotted against test voltage. (**C**) Peak current amplitudes measured at a test voltage of 0 mV; numbers of oocytes (*n*) indicated. (**D**) Normalized conductance (G_{norm})-voltage plots and Boltzmann analysis. (**E**) Currents during a 2.5 s test pulse to +40 mV normalized to peak and overlaid. (**F**) Time constant obtained with double-exponential fitting (black and grey bars) and the relative current at the end of the test pulse ($I_{2.5s}/I_{peak}$, empty bars); numbers of oocytes (*n*) indicated. (**G**) Area under the original current traces (i.e. charge at +40 mV during 2.5 s). (**H**) Voltage dependence of steady-state inactivation (data were fitted with a single Boltzmann function). (**I**) Kinetics of recovery from inactivation (data were fitted with a single or a double-exponential function).

mutations leads to a loss of CSI in the heteromeric WT + mutant ternary configuration, each of them specifically modifies CSI on and off rates of the channel complex (Supplementary Material, Fig. S4).

LOF and GOF in a native setting

Native Kv4 channels form complexes with auxiliary KChIPs and DPPs, both known to enhance channel surface expression and to specifically modify channel gating (26,28). In fact, Kv4 channels

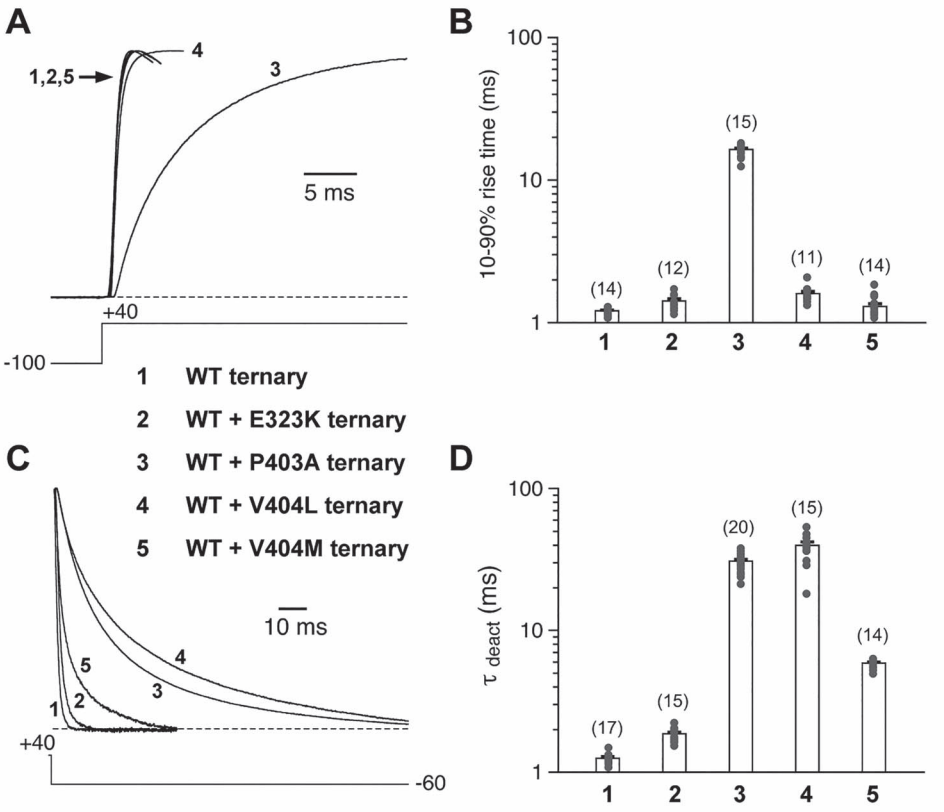

Figure 6. Kinetic analysis of activation and deactivation for Kv4.2 WT and heteromeric WT + mutant ternary complexes. Homomeric WT and heteromeric WT + mutant Kv4.2 channels were studied in a ternary configuration with KChIP2 and DPP6. The data are marked by numbers: (1) WT ternary; (2) WT + E323K ternary; (3) WT + P403A ternary; (4) WT + V404L ternary; (5) WT + V404M ternary. (**A**) Current rising phase at +40 mV; (**B**) 10–90% rise times; (**C**) tail current relaxation at −60 mV; (**D**) deactivation time constants; numbers of oocytes (*n*) indicated.

in many neurons are likely to be ternary complexes containing both types of auxiliary β-subunits (25,40,41). Thus, apparently low expression levels and/or conspicuous gating properties observed for a channel mutant, if examined in isolation, may be pushed into the background if auxiliary β-subunits are present, provided the mutation itself does not affect the interaction. Here, we chose KChIP2 and DPP6 splice variants abundantly expressed in the hippocampus (30,42,43) for auxiliary β-subunit co-expression. Our finding that for both Kv4.2 WT and all tested mutants, β-subunit co-expression causes a significant increase in peak current amplitude suggests that the mutants are still able to interact with auxiliary β-subunits, although in some cases the effects of the β-subunits on channel gating are absent or differ from those observed for Kv4.2 WT. These special mutant features were not further examined in the present study.

Instead, the Kv4.2 mutants were tested in a heteromeric ternary configuration (see Figs 5 and 6), to judge the likely pathogenicity of the corresponding heterozygous *KCND2* variants in our cohort of individuals. The significantly reduced peak current amplitudes found for WT + E323K ternary and WT + P403A may be classified as partial LOF; however, the current amplitudes measured in a heterologous expression system must be interpreted with caution, and immunocytochemical analysis suggested equal amounts of membrane protein for WT ternary, WT + E323K ternary and WT + P403A ternary (data not shown). For WT + E323K ternary, all other modifications (tentatively GOF; see Supplementary Material, Tables S1 and S2) failed to reach significance. WT + P403A ternary shows further signs of partial LOF: the persistently slowed kinetics and positively shifted voltage dependence of activation and the slowed recovery kinetics. However, WT + P403A ternary also exhibits GOF features, namely slowed and incomplete macroscopic inactivation combined with slowed deactivation and a positively shifted voltage dependence of inactivation. Similarly, WT + V404L ternary exhibits both partial LOF (steepened voltage dependence of inactivation and slowed recovery kinetics) and GOF features (slowed and incomplete macroscopic inactivation combined with slowed deactivation and negatively shifted as well as steepened voltage dependence of activation), whereas V404M exhibits only GOF features (incomplete macroscopic inactivation combined with slowed deactivation and negatively shifted voltage dependence of activation) in the heteromeric ternary configuration (see also Supplementary Material, Tables S1 and S2).

The crucial question to be asked is whether and how the LOF and GOF features observed for the individual mutants in a native setting may influence cellular neurophysiology and/or neurodevelopmental aspects. Certainly, the most striking LOF feature observed in our study is the persistently impaired activation of WT + P403A ternary, which is very likely to suppress I_{SA}. The I_{SA} suppression is expected to compromise the control of dendritic excitation, including facilitated generation and back-propagation of action potentials, constitutive frequency-independent spike broadening and reduced dampening of excitatory postsynaptic potentials (9–12; possibly in cases 1–3). The most striking GOF feature, observed equally for WT + P403A

ternary, WT + V404L ternary and WT + V404M ternary in our study, albeit with quantitative differences, is the slowed and/or incomplete current relaxation at all voltages, presumably caused by slowed channel closure. In affected neurons, this feature is expected to cause an increase in potassium conductance and, thus, hyperpolarization of the resting membrane potential for tens to hundreds of milliseconds following one or more action potentials. Due to putatively very slow I_{SA} activation kinetics, P403A expressing neurons may show this behavior only following an extended spike train (possibly in cases 2 and 3), whereas in V404L and V404M expressing neurons a single spike may be sufficient to cause an unphysiological pause in electrical activity (possibly in cases 4–6). Thus, due to the fast activation and extremely slow deactivation kinetics of WT + V404L ternary, V404L expressing neurons (cases 4 and 5) might be most prominently affected.

Potassium channel dysfunction of genetic origin may cause epilepsy and neurodevelopmental disorders including autism (7,44). The disease-related Kv channel gene families (and affected types of α-subunit) include *KCNA* (Kv1), *KCNB* (Kv2), *KCNC* (Kv3), *KCND* (Kv4), *KCNQ* (Kv7), *KCNV* (Kv8) and *KCNH* (Kv10; (7); see also Supplementary Material, Fig. S1). Although the majority of pathogenic Kv channel gene variants causing neurological disorders associated with epilepsy exhibits LOF, we currently see a growing number of GOF variants associated with epilepsy; i.e. enhanced intrinsic Kv channel activity may lead to network hyperexcitability (45).[1] This seemingly paradoxical finding may be explained by one or more of the following pathogenic mechanisms: (1) Kv channel GOF and reduced intrinsic excitability in inhibitory interneurons may lead to hyperexcitability in postsynaptic neurons (disinhibition); (2) Kv channel GOF and a resultant strong (after-) hyperpolarization following an action potential may particularly well remove sodium channel inactivation, thereby leading to facilitated action potential firing; (3) Kv channel GOF leading to reduced activity of a neuron may increase the number of synapses and/or the number of postsynaptic glutamate receptors (homeostatic plasticity) (45). The mechanism of disinhibition has been suggested as an explanation for the occurrence of epileptic seizures in the reported twin boys carrying the V404M variant (34) and may thus also apply to cases 4–6 of the present study, in which epileptic seizures were observed (see Table 1). More recently, membrane hyperpolarization and reduced excitability due to potassium channel GOF have been linked to developmental disorders associated for instance with impaired cell migration, which may eventually lead to neuroanatomical abnormalities and neurodevelopmental disorders as well as numerous non-neuronal dysmorphic physical features (46). Although the *KCND* (Kv4) subfamily of Kv channel genes has thus far received little attention in this context, the latter mechanism may explain how Kv4.2 channel GOF due to the *KCND2* variants described herein can lead to multi-domain GDD (cases 1–6; see Table 1).

KCND2 variants and clinical phenotypes

The first *KCND2* variant associated with a neurological phenotype was a paternally inherited deletion found in a female with refractory temporal lobe epilepsy starting at the age of 13 years, with no histological abnormalities, but cognitive impairment preceding her history of epilepsy (47). In that individual, a 5 bp deletion leads to a frameshift and a premature stop codon, and the resultant mutant Kv4.2 protein is predicted to lack the last 44 amino acids (N587fsX1). The observed partial LOF may be attributed to the loss of multiple extracellular signal receptor kinase phosphorylation sites (48) and the loss of interaction motifs for the cytoskeletal proteins filamin (49) and postsynaptic density 95 (PSD-95) (50), both located within this C-terminal region (47). Thus, there is neither genetic nor mechanistic overlap of the N587fsX1 individual with our cohort. Since that individual shows cognitive impairment and did not show epileptic seizures under the age of 13 years, a phenotypic overlap with our cohort at a later stage cannot be excluded; however, she did apparently not show GDD (47). The same may apply to a reported *KCND1* nonsense variant associated with a similar C-terminal truncation detected in a male with epilepsy onset at the age of 8 years and normal intellectual development (51).

More recently, a heterozygous *KCND2* missense variant has been identified, which is genetically identical to the variant identified in case 6 of our study (V404M). It was discovered in monozygotic twin boys presenting with early-onset (at the age of 2 months) intractable seizures, autism, language disability and an overall cognitive functioning in the very low range (34). Similarly, early disease onset and delayed speech and cognitive development are common phenotypic features in the cohort of individuals described herein (see Table 1). Moreover, within our cohort, all three cases with *KCND2* variants affecting V404 (V404L in cases 4 and 5 and V404M in case 6) exhibit severe epilepsy, while this phenotype has not been noted in the other three individuals (cases 1–3, see Table 1). Notably, in cases 4–6, the *KCND2* variants are associated with net GOF, whereas in cases 1–3 both LOF and GOF features can be found (see Supplementary Material, Tables S1 and S2). Our results suggest that *KCND2* (Kv4.2) GOF rather than LOF variants, associated with the identified mutational 'hotspots' (S4S5 linker and distal S6), favor epileptic seizure susceptibility.

In our study, autism was only observed in case 4 (V404L), but not for the other five cases, including the one carrying the previously published V404M variant (34) (see Table 1, case 6). Just like the autistic identical twin boys harboring the V404M variant (34), our V404L individual with autism (case 4) is male, whereas our V404M individual (case 6) is female. The absence of autism in case 6 may reflect the generally found lower probability for females to be diagnosed with autism (52). Notably, the identical twins with autism harboring the V404M variant also share variants of other genes besides *KCND2*, including *BICC1* (coding for an RNA binding protein), *GPR124* (coding for a G-protein-coupled receptor) and *SLC8A2* (coding for a sodium/calcium exchanger) (34). Thus, autism may not represent a key phenotypic feature associated with *KCND2* variants. On the other hand, our data suggest that delayed motor development and muscle hypotonia are key features of *KCND2* missense variants (see Table 1), although these features were not reported for the identical twins harboring the V404M variant (34). Apparently, the clinical phenotypes associated with heterozygous *KCND2* missense variants are highly variable. Which of the different phenotypic features (GDD, autism or epileptic seizures) is dominant may depend on the relative proportion of LOF and GOF mutational effects. Moreover, additional gene variants and other factors, including sex (52), may modify *KCND2*-associated phenotypes.

Pharmacological interventions in developmental epileptic encephalopathy are usually based on inhibition of excitatory ligand and voltage-dependent ion channels, inhibition of excitatory neurotransmitter release and/or potentiation of

1 Ref. 45: In this review article the V404M variant reported by Lee and co-workers (34) is erroneously referred to as V404I.

GABAergic effects, as evident from the medications applied in cases 4–6 of our cohort (53); (see also Supplementary Material, Clinical Reports). Based on the knowledge gained from the genetic and biophysical analyses performed in the present study, a more specific and presymptomatic pharmacological intervention, possibly one which directly targets Kv4.2 channels in an appropriate manner, would be desirable. In particular, considering neurodevelopmental disorders associated with *KCND2* (Kv4.2) GOF, Kv4.2 channel inhibition in early childhood may be an option to be considered. Pharmacological compounds with intriguing properties, including toxins isolated from various tarantula (54,55) and scorpion venoms (56,57), may serve as lead structures. The tarantula toxins inhibit Kv4 channels by gating modification including a positive shift in the activation curve (54,55), a feature that may target predominantly the subthreshold active neuronal I_{SA} rather than cardiac I_{to}. The scorpion toxins selectively inhibit Kv4 channels with DPPs bound (56), a combination found predominantly in the brain. These compounds and newly developed ones should be explored in more detail to address their effectivity in neuronal and their tolerability in cardiac tissue. It would be desirable if they may eventually allow for early mechanism-based precision medicine to benefit young individuals and minimize developmental disturbances.

Materials and Methods

Individuals and genomic analysis

Research subjects. Written informed consent for all subjects was obtained in accordance with protocols approved by the respective ethics committees of the institutions involved in this study.

Genetic analysis. Some of the investigators presenting affected individuals in this study were connected through GeneMatcher, a web-based tool for researchers and clinicians working on identical genes (58). The different centers involved in this study utilized comparable protocols for DNA isolation, whole-exome and -genome sequencing, bioinformatics processing and variant interpretation. For cases 2 and 4, sequencing and data analysis was performed by the Genomics Platform at the Broad Institute of MIT and Harvard and the Senckenberg Centre for Human Genetics, respectively. The *KCND2* variant of case 6 was identified via targeted-gene panel analysis.

Structural modeling

Structural homology modeling based on the crystal structure coordinates of a Kv1.2-Kv2.1 chimera (PDB accession number 2R9R); (59) was performed with PyMol (Schrödinger, New York NY). Amino acid substitutions were simulated considering the most likely backbone-dependent rotamer orientation, and the putative steric consequences of the amino acid substitution within a distance of 8 Å were taken into account.

Plasmids and *in vitro* transcription

KCND2 variants were inserted into a pGEM-HE vector containing the complete coding region of the human Kv4.2 cDNA (60) utilizing the Q5® Site-Directed Mutagenesis Kit (New England Biolabs, Ipswich MA) and verified by Sanger sequencing. For auxiliary β-subunit co-expression, we used the human KChIP2b splice variant (previously referred to as KChIP2.1; 27) in pGEM-HE and the human DPP6s splice variant (also referred to as DPPX-S) (61) (gift from Henry Jerng, Baylor College of Medicine, Houston, TX) in a pUC-derivative. Transformed JM109 *Escherichia coli* cells (Promega, Fitchburg WI) were grown in Luria Broth medium complemented with ampicillin, and plasmids were isolated using the QIAprep Spin Miniprep Kit (QIAGEN, Hilden, Germany). Purified plasmids were linearized using *Not*I (New England Biolabs), and the RiboMaxLargeScale RNA production system T7 (Promega) was utilized to *in vitro* transcribe cRNAs.

Heterologous channel expression

Kv4.2 channels were expressed in *Xenopus laevis* oocytes as described previously (23,38). To express homomeric Kv4.2 channels, 5 ng total cRNA were injected per oocyte. For heteromeric channel expression, Kv4.2 WT and mutant cRNAs were injected at a ratio of either 1:1 (2.5 + 2.5 ng per oocyte) or 1:4 (1 + 4 ng per oocyte). Both Kv4.2 WT and mutant homomers were co-expressed with KChIP2 (5 ng cRNA per oocyte) or DPP6 (5 ng cRNA per oocyte). Furthermore, Kv4.2 WT homomers (5 ng cRNA per oocyte) and Kv4.2 WT + mutant heteromers (2.5 + 2.5 ng cRNA per oocyte) were co-expressed with both KChIP2 and DPP6 (both 5 ng cRNA per oocyte) for ternary complex formation. Oocytes were used for electrophysiological recordings 1–3 days after cRNA injection.

Recording techniques and pulse protocols

Currents were recorded at room temperature (20–22°C) under two-electrode voltage clamp as described previously (23,38) using TurboTec amplifiers (npi, Tamm, Germany) controlled by PatchMaster software (HEKA, Lambrecht, Germany). To minimize contamination of small-sized Kv4.2-mediated outward currents at depolarized membrane potentials by endogenous chloride currents, we used a low chloride (15 mM) bath solution in most experiments containing (in mM) 7.4 NaCl, 88.6 Na-aspartate, 2 KCl, 1.8 $CaCl_2$, 1 $MgCl_2$ and 5 HEPES, pH 7.4 with NaOH. For oocytes expressing ternary complexes, the same solution was used with Na-aspartate replaced by NaCl. Pulse protocols are explained in the figure legends. Capacitive current transients were not compensated, and the current measured at −95 mV (approximate E_{rev} for K^+) was used to calculate the leak current at any other voltage. For the study of activation kinetics of ternary complexes, a p/5 protocol was used for leak subtraction.

Data analysis

Data were analysed using FitMaster (HEKA) and Kaleidagraph (Synergy Software, Reading PA). The voltage dependence of activation was analysed based on cord conductances (calculated with $E_{rev} = -95$ mV) and a fourth-order Boltzmann function as described previously (23,38). Macroscopic activation kinetics was described by the 10–90% rise time (Supplementary Material, Fig. S2), and macroscopic inactivation kinetics were approximated by a double-exponential function. In addition, the remaining current at the end of a 2.5 s test pulse relative to peak was determined. Deactivating tail current kinetics (at −60 mV) was approximated by a single-exponential function. The voltage dependence of steady-state inactivation was analysed based on a single or, if necessary, the sum of two Boltzmann functions. Recovery from inactivation (at −100 mV) was described by a single- or, if necessary, a double-exponential function. The biphasic nature of the voltage dependence of steady-state inactivation and recovery kinetics observed for some channels were not further studied, and the analysis was restricted to

the more negative and the faster components, respectively. Pooled data are presented as mean ± SEM, and individual data points are shown for summary bar graphs. Statistical analyses for multiple groups are based on one-way analysis of variance with Dunnett's *post hoc* testing and for two groups on Student's *t*-test. Data and statistical analysis results are summarized in Supplementary Material, Tables S1 and S2.

Supplementary Material

Supplementary Material is available at *HMG* Online.

Acknowledgements

We thank the family members for their participation and collaboration. This study makes use of data generated by the DECIPHER community (62). A full list of centers that contributed to the generation of the data is available from http://decipher.sanger.ac.uk and via email from decipher@sanger.ac.uk. We thank Telse Kock and Jessica Wollberg for the cloning of Kv4.2 mutant constructs.

Conflict of Interest statement. None declared.

Funding

This work was supported by the Deutsche Forschungsgemeinschaft (BA2055/1-3 and BA2055/6-1 to R.B., HE8155/1-1 to U.B.S.H., LE1030/16-1 to H.L.) and the China Scholarship Council (201806090432). H.M. is an employee and shareholder at Invitae Corporation. Sequencing and analysis (case 2) was provided by the Broad Institute of MIT and Harvard Center for Mendelian Genomics (Broad CMG) and was funded by the National Human Genome Research Institute, the National Eye Institute and the National Heart, Lung and Blood Institute grants (UM1 HG008900, R01 HG009141) and by the Chan Zuckerberg Initiative to the Rare Genomes Project. Funding for the DECIPHER project was provided by the Wellcome Trust.

References

1. Shevell, M. (2008) Global developmental delay and mental retardation or intellectual disability: conceptualization, evaluation, and etiology. *Pediatr. Clin. N. Am.*, **55**, 1071–1084.
2. Shevell, M., Ashwal, S., Donley, D., Flint, J., Gingold, M., Hirtz, D., Majnemer, A., Noetzel, M. and Sheth, R.D. (2003) Practice parameter: evaluation of the child with global developmental delay: report of the quality standards Subcommittee of the American Academy of neurology and the practice Committee of the Child Neurology Society. *Neurology*, **60**, 367–380.
3. Mithyantha, R., Kneen, R., McCann, E. and Gladstone, M. (2017) Current evidence-based recommendations on investigating children with global developmental delay. *Arch. Dis. Child.*, **102**, 1071–1076.
4. Vasudevan, P. and Suri, M. (2017) A clinical approach to developmental delay and intellectual disability. *Clin. Med.*, **17**, 558–561.
5. Srour, M. and Shevell, M. (2014) Genetics and the investigation of developmental delay/intellectual disability. *Arch. Dis. Child.*, **99**, 386–389.
6. Deciphering Developmental Disorders, S. (2017) Prevalence and architecture of de novo mutations in developmental disorders. *Nature*, **542**, 433–438.
7. Allen, N.M., Weckhuysen, S., Gorman, K., King, M.D. and Lerche, H. (2020) Genetic potassium channel-associated epilepsies: clinical review of the Kv family. *Eur. J. Paediatr. Neurol.*, **24**, 105–116.
8. Serodio, P., Kentros, C. and Rudy, B. (1994) Identification of molecular components of A-type channels activating at subthreshold potentials. *J. Neurophysiol.*, **72**, 1516–1529.
9. Kim, J., Wei, D.S. and Hoffman, D.A. (2005) Kv4 potassium channel subunits control action potential repolarization and frequency-dependent broadening in rat hippocampal CA1 pyramidal neurones. *J. Physiol.*, **569**, 41–57.
10. Hoffman, D.A., Magee, J.C., Colbert, C.M. and Johnston, D. (1997) K^+ channel regulation of signal propagation in dendrites of hippocampal pyramidal neurons. *Nature*, **387**, 869–875.
11. Ramakers, G.M. and Storm, J.F. (2002) A postsynaptic transient K^+ current modulated by arachidonic acid regulates synaptic integration and threshold for LTP induction in hippocampal pyramidal cells. *Proc. Natl. Acad. Sci. U. S. A.*, **99**, 10144–10149.
12. Watanabe, S., Hoffman, D.A., Migliore, M. and Johnston, D. (2002) Dendritic K^+ channels contribute to spike-timing dependent long-term potentiation in hippocampal pyramidal neurons. *Proc. Natl. Acad. Sci. U. S. A.*, **99**, 8366–8371.
13. Bernard, C., Anderson, A., Becker, A., Poolos, N.P., Beck, H. and Johnston, D. (2004) Acquired dendritic channelopathy in temporal lobe epilepsy. *Science*, **305**, 532–535.
14. Castro, P.A., Cooper, E.C., Lowenstein, D.H. and Baraban, S.C. (2001) Hippocampal heterotopia lack functional Kv4.2 potassium channels in the methylazoxymethanol model of cortical malformations and epilepsy. *J. Neurosci.*, **21**, 6626–6634.
15. Francis, J., Jugloff, D.G., Mingo, N.S., Wallace, M.C., Jones, O.T., Burnham, W.M. and Eubanks, J.H. (1997) Kainic acid-induced generalized seizures alter the regional hippocampal expression of the rat Kv4.2 potassium channel gene. *Neurosci. Lett.*, **232**, 91–94.
16. Lugo, J.N., Barnwell, L.F., Ren, Y., Lee, W.L., Johnston, L.D., Kim, R., Hrachovy, R.A., Sweatt, J.D. and Anderson, A.E. (2008) Altered phosphorylation and localization of the A-type channel, Kv4.2 in status epilepticus. *J. Neurochem.*, **106**, 1929–1940.
17. Monaghan, M.M., Menegola, M., Vacher, H., Rhodes, K.J. and Trimmer, J.S. (2008) Altered expression and localization of hippocampal A-type potassium channel subunits in the pilocarpine-induced model of temporal lobe epilepsy. *Neuroscience*, **156**, 550–562.
18. Su, T., Cong, W.D., Long, Y.S., Luo, A.H., Sun, W.W., Deng, W.Y. and Liao, W.P. (2008) Altered expression of voltage-gated potassium channel 4.2 and voltage-gated potassium channel 4-interacting protein, and changes in intracellular calcium levels following lithium-pilocarpine-induced status epilepticus. *Neuroscience*, **157**, 566–576.
19. Tsaur, M.L., Sheng, M., Lowenstein, D.H., Jan, Y.N. and Jan, L.Y. (1992) Differential expression of K^+ channel mRNAs in the rat brain and down-regulation in the hippocampus following seizures. *Neuron*, **8**, 1055–1067.
20. Swartz, K.J. (2004) Towards a structural view of gating in potassium channels. *Nat. Rev. Neurosci.*, **5**, 905–916.
21. Lu, Z., Klem, A.M. and Ramu, Y. (2002) Coupling between voltage sensors and activation gate in voltage-gated K^+ channels. *J. Gen. Physiol.*, **120**, 663–676.
22. Yifrach, O. and MacKinnon, R. (2002) Energetics of pore opening in a voltage-gated K^+ channel. *Cell*, **111**, 231–239.

23. Barghaan, J. and Bähring, R. (2009) Dynamic coupling of voltage sensor and gate involved in closed-state inactivation of Kv4.2 channels. *J. Gen. Physiol.*, **133**, 205–224.
24. Jerng, H.H., Shahidullah, M. and Covarrubias, M. (1999) Inactivation gating of Kv4 potassium channels: molecular interactions involving the inner vestibule of the pore. *J. Gen. Physiol.*, **113**, 641–660.
25. Maffie, J. and Rudy, B. (2008) Weighing the evidence for a ternary protein complex mediating A-type K^+ currents in neurons. *J. Physiol.*, **586**, 5609–5623.
26. An, W.F., Bowlby, M.R., Betty, M., Cao, J., Ling, H.P., Mendoza, G., Hinson, J.W., Mattsson, K.I., Strassle, B.W., Trimmer, J.S. *et al.* (2000) Modulation of A-type potassium channels by a family of calcium sensors. *Nature*, **403**, 553–556.
27. Bähring, R., Dannenberg, J., Peters, H.C., Leicher, T., Pongs, O. and Isbrandt, D. (2001) Conserved Kv4 N-terminal domain critical for effects of Kv channel-interacting protein 2.2 on channel expression and gating. *J. Biol. Chem.*, **276**, 23888–23894.
28. Nadal, M.S., Ozaita, A., Amarillo, Y., de Miera, E.V., Ma, Y., Mo, W., Goldberg, E.M., Misumi, Y., Ikehara, Y., Neubert, T.A. *et al.* (2003) The CD26-related dipeptidyl aminopeptidase-like protein DPPX is a critical component of neuronal A-type K^+ channels. *Neuron*, **37**, 449–461.
29. Shibata, R., Misonou, H., Campomanes, C.R., Anderson, A.E., Schrader, L.A., Doliveira, L.C., Carroll, K.I., Sweatt, J.D., Rhodes, K.J. and Trimmer, J.S. (2003) A fundamental role for KChIPs in determining the molecular properties and trafficking of Kv4.2 potassium channels. *J. Biol. Chem.*, **278**, 36445–36454.
30. Zagha, E., Ozaita, A., Chang, S.Y., Nadal, M.S., Lin, U., Saganich, M.J., McCormack, T., Akinsanya, K.O., Qi, S.Y. and Rudy, B. (2005) DPP10 modulates Kv4-mediated A-type potassium channels. *J. Biol. Chem.*, **280**, 18853–18861.
31. Beck, E.J., Bowlby, M., An, W.F., Rhodes, K.J. and Covarrubias, M. (2002) Remodelling inactivation gating of Kv4 channels by KChIP1, a small-molecular-weight calcium-binding protein. *J. Physiol.*, **538**, 691–706.
32. Jerng, H.H., Qian, Y. and Pfaffinger, P.J. (2004) Modulation of Kv4.2 channel expression and gating by dipeptidyl peptidase 10 (DPP10). *Biophys. J.*, **87**, 2380–2396.
33. Isbrandt, D., Leicher, T., Waldschütz, R., Zhu, X., Luhmann, U., Michel, U., Sauter, K. and Pongs, O. (2000) Gene structures and expression profiles of three human *KCND* (Kv4) potassium channels mediating A-type currents I_{TO} and I_{SA}. *Genomics*, **64**, 144–154.
34. Lee, H., Lin, M.C., Kornblum, H.I., Papazian, D.M. and Nelson, S.F. (2014) Exome sequencing identifies de novo gain of function missense mutation in KCND2 in identical twins with autism and seizures that slows potassium channel inactivation. *Hum. Mol. Genet.*, **23**, 3481–3489.
35. Lin, M.A., Cannon, S.C. and Papazian, D.M. (2018) Kv4.2 autism and epilepsy mutation enhances inactivation of closed channels but impairs access to inactivated state after opening. *Proc. Natl. Acad. Sci. U. S. A.*, **115**, E3559–E3568.
36. Bähring, R. and Covarrubias, M. (2011) Mechanisms of closed-state inactivation in voltage-gated ion channels. *J. Physiol.*, **589**, 461–479.
37. Harpaz, Y., Gerstein, M. and Chothia, C. (1994) Volume changes on protein folding. *Structure*, **2**, 641–649.
38. Wollberg, J. and Bähring, R. (2016) Intra- and intersubunit dynamic binding in Kv4.2 channel closed-state inactivation. *Biophys. J.*, **110**, 157–175.
39. Bähring, R., Barghaan, J., Westermeier, R. and Wollberg, J. (2012) Voltage sensor inactivation in potassium channels. *Front. Pharmacol.*, **3**, 1–8.
40. Amarillo, Y., De Santiago-Castillo, J.A., Dougherty, K., Maffie, J., Kwon, E., Covarrubias, M. and Rudy, B. (2008) Ternary Kv4.2 channels recapitulate voltage-dependent inactivation kinetics of A-type K^+ channels in cerebellar granule neurons. *J. Physiol.*, **586**, 2093–2106.
41. Jerng, H.H., Kunjilwar, K. and Pfaffinger, P.J. (2005) Multiprotein assembly of Kv4.2, KChIP3 and DPP10 produces ternary channel complexes with I_{SA}-like properties. *J. Physiol.*, **568**, 767–788.
42. Nadal, M.S., Amarillo, Y., de Miera, E.V. and Rudy, B. (2006) Differential characterization of three alternative spliced isoforms of DPPX. *Brain Res.*, **1094**, 1–12.
43. Rhodes, K.J., Carroll, K.I., Sung, M.A., Doliveira, L.C., Monaghan, M.M., Burke, S.L., Strassle, B.W., Buchwalder, L., Menegola, M., Cao, J. *et al.* (2004) KChIPs and Kv4 α subunits as integral components of A-type potassium channels in mammalian brain. *J. Neurosci.*, **24**, 7903–7915.
44. Guglielmi, L., Servettini, I., Caramia, M., Catacuzzeno, L., Franciolini, F., D'Adamo, M.C. and Pessia, M. (2015) Update on the implication of potassium channels in autism: K^+ channel autism spectrum disorder. *Front. Cell. Neurosci.*, **9**, 1–14.
45. Niday, Z. and Tzingounis, A.V. (2018) Potassium channel gain of function in epilepsy: An unresolved paradox. *Neuroscientist*, **24**, 368–380.
46. Hamilton, M.J. and Suri, M. (2020) "electrifying dysmorphology": potassium channelopathies causing dysmorphic syndromes. *Adv. Genet.*, **105**, 137–174.
47. Singh, B., Ogiwara, I., Kaneda, M., Tokonami, N., Mazaki, E., Baba, K., Matsuda, K., Inoue, Y. and Yamakawa, K. (2006) A Kv4.2 truncation mutation in a patient with temporal lobe epilepsy. *Neurobiol. Dis.*, **24**, 245–253.
48. Schrader, L.A., Birnbaum, S.G., Nadin, B.M., Ren, Y., Bui, D., Anderson, A.E. and Sweatt, J.D. (2006) ERK/MAPK regulates the Kv4.2 potassium channel by direct phosphorylation of the pore-forming subunit. *Am. J. Physiol. Cell Physiol.*, **290**, C852–C861.
49. Petrecca, K., Miller, D.M. and Shrier, A. (2000) Localization and enhanced current density of the Kv4.2 potassium channel by interaction with the actin-binding protein filamin. *J. Neurosci.*, **20**, 8736–8744.
50. Wong, W., Newell, E.W., Jugloff, D.G., Jones, O.T. and Schlichter, L.C. (2002) Cell surface targeting and clustering interactions between heterologously expressed PSD-95 and the *Shal* voltage-gated potassium channel, Kv4.2. *J. Biol. Chem.*, **277**, 20423–20430.
51. Miao, P., Feng, J., Guo, Y., Wang, J., Xu, X., Wang, Y., Li, Y., Gao, L., Zheng, C. and Cheng, H. (2018) Genotype and phenotype analysis using an epilepsy-associated gene panel in Chinese pediatric epilepsy patients. *Clin. Genet.*, **94**, 512–520.
52. Ferri, S.L., Abel, T. and Brodkin, E.S. (2018) Sex differences in autism spectrum disorder: a review. *Curr. Psychiatry Rep.*, **20**, 9.
53. Shbarou, R. (2016) Current treatment options for early-onset pediatric epileptic encephalopathies. *Curr. Treat. Options Neurol.*, **18**, 44.
54. Ebbinghaus, J., Legros, C., Nolting, A., Guette, C., Celerier, M.L., Pongs, O. and Bähring, R. (2004) Modulation of Kv4.2 channels by a peptide isolated from the venom of the giant bird-eating tarantula Theraphosa leblondi. *Toxicon*, **43**, 923–932.

55. Sanguinetti, M.C., Johnson, J.H., Hammerland, L.G., Kelbaugh, P.R., Volkmann, R.A., Saccomano, N.A. and Mueller, A.L. (1997) Heteropodatoxins: peptides isolated from spider venom that block Kv4.2 potassium channels. *Mol. Pharmacol.*, **51**, 491–498.
56. Maffie, J.K., Dvoretskova, E., Bougis, P.E., Martin-Eauclaire, M.F. and Rudy, B. (2013) Dipeptidyl-peptidase-like-proteins confer high sensitivity to the scorpion toxin AmmTX3 to Kv4-mediated A-type K^+ channels. *J. Physiol.*, **591**, 2419–2427.
57. Vacher, H., Diochot, S., Bougis, P.E., Martin-Eauclaire, M.F. and Mourre, C. (2006) Kv4 channels sensitive to BmTX3 in rat nervous system: autoradiographic analysis of their distribution during brain ontogenesis. *Eur. J. Neurosci.*, **24**, 1325–1340.
58. Sobreira, N., Schiettecatte, F., Valle, D. and Hamosh, A. (2015) GeneMatcher: a matching tool for connecting investigators with an interest in the same gene. *Hum. Mutat.*, **36**, 928–930.
59. Long, S.B., Tao, X., Campbell, E.B. and MacKinnon, R. (2007) Atomic structure of a voltage-dependent K^+ channel in a lipid membrane-like environment. *Nature*, **450**, 376–382.
60. Zhu, X.-R., Wulf, A., Schwarz, M., Isbrandt, D. and Pongs, O. (1999) Characterization of human Kv4.2 mediating a rapidly-inactivating transient voltage-sensitive K^+ current. *Recept. Channels*, **6**, 387–400.
61. Wada, K., Yokotani, N., Hunter, C., Doi, K., Wenthold, R.J. and Shimasaki, S. (1992) Differential expression of two distinct forms of mRNA encoding members of a dipeptidyl aminopeptidase family. *Proc. Natl. Acad. Sci. U. S. A.*, **89**, 197–201.
62. Firth, H.V., Richards, S.M., Bevan, A.P., Clayton, S., Corpas, M., Rajan, D., Van Vooren, S., Moreau, Y., Pettett, R.M. and Carter, N.P. (2009) DECIPHER: database of chromosomal imbalance and phenotype in humans using Ensembl resources. *Am. J. Hum. Genet.*, **84**, 524–533.